Hydrogeophysical Analysis of Vertical Electrical Soundings for Groundwater Potential and Aquifer Vulnerability Evaluation in the Federal Capital Territory, Abuja, Nigeria

Ibrahim, D., * Nemoto, T. and Raghavan, V.
Department of Geosciences, Osaka Metropolitan University, Japan
E-mail: sp23519y@st.omu.ac.jp*
**Corresponding Author*

DOI: https://doi.org/10.52939/ijg.v21i1.3797

Abstract
A report from the United Nations indicates that groundwater accounts for 26% of the world's renewable freshwater and is critical for over 2.5 billion people. Expanding groundwater exploitation and management is essential to obtaining universal access to clean water and meeting the 2030 Sustainable Development Goals (SDGs), especially in Nigeria's capital, Abuja. The Water shortage in the region is caused by population increase and urbanization, with most of the potable water coming from hand-dug wells and boreholes. This study aims to identify Abuja's groundwater potential and aquifer vulnerability zones by utilizing Hydrogeophysical methodology in the form of Vertical Electrical Sounding (VES) and Geographic Information System (GIS). Geologically, the area is dominated by Precambrian rocks and sedimentary formations, including critical lithologic units such as Older Granites, Metasediments/Metavolcanics, Migmatite-Gneiss Complex, and Nupe Sandstones. VES data were acquired from 823 sites using the Schlumberger electrode configuration with maximum electrode spacing (AB/2) of 100m and processed with IPI2Win software to determine the subsurface geoelectrical layers. Crucial parameters such as Depth to Bedrock (DB), the Dar-Zarrouk Parameters (DZP), and layer resistivity were determined. Vulnerability assessment was carried out using longitudinal conductance. Consequently, most of the study area indicates moderate protective capacity. The Reflection Coefficient (RC) varies from -0.996 to 0.999, while the protective capacity ranges from poor (<0.10) to very good (5-10). Based on the DB and RC, the groundwater potential zone of the area was determined. Very low (DB < 13m and RC < 0.8), Low (DB < 13m and RC > 0.8), Moderate (DB ≥ 13m and RC > 0.8), High (DB ≥ 13m and RC < 0.8) and Very High (DB ≥ 30m and RC < 0.8). Maps were generated in the QGIS environment using the Kriging interpolation method. This result will promote sustainable management of groundwater in the study area.

Keywords: Aquifer Vulnerability, Groundwater Potential Zones, Geoelectrical Resistivity, Kriging Interpolation, Vertical Electrical Sounding (VES)

1. Introduction

Groundwater is one of the most treasured resources on earth; the socio-economic condition and growth of regions depend mainly on the availability of water [1]. In the past, civilizations have grown according to the availability of freshwater. It is anticipated that the supply of fresh water for human needs may become severely constrained in the future due to the expanding global population and climate change. The importance of sustainable groundwater management and development cannot be overemphasized, especially in Sub-Saharan Africa, where Nigeria is situated. The only practical means of supplying water to dispersed rural populations in vast regions of Africa, South America, and Asia is groundwater; alternative water supplies are often expensive and unreliable to develop [2]. More than 90% of the rural population globally depends on groundwater for irrigation, drinking, and other domestic activities. Urbanization, industrialization, and population growth are the leading causes of the decline in the amount of water resources accessible. Despite the importance of this resource, its quality is crucial for healthy living. Climate, local geology, topography, interaction of rock and water, and anthropogenic activity are among the numerous variables that affect the quality of groundwater [3].

The impact of climate change on groundwater resources in Africa is expected to be relatively smaller when compared to non-climatic drivers, such as population and urbanization growth. Groundwater supplies nearly 73% of drinking water in rural areas and 45% in urban areas of Nigeria [4]. Determining areas with promising groundwater potential is only possible through groundwater potential zone mapping. It involves integrating, processing, and analyzing geological, hydrological, climatic, and environmental data to identify areas where fresh groundwater can be efficiently tapped or managed. It is crucial for managing groundwater resources sustainably, particularly in regions severely short on water or experiencing significant population expansion. This knowledge helped to inform decisions about where best to place groundwater development infrastructure and how the resources may be managed sustainably into the future. Groundwater Vulnerability refers to the relative possibility that a contaminant introduced to the land surface will pass through an unsaturated zone and reach groundwater or aquifer [5]. Creating vulnerability maps is one method for implementing measures to protect groundwater. This approach enables proactive or corrective land use management to safeguard this valuable resource.

The Federal Capital Territory (FCT) Abuja is Nigeria's eighth-most populous city. Political, economic, and social factors drive population growth, resulting in a reported 400% population increase between 2000 and 2020. One of the major concerns for developing nations is providing safe, potable water to the populace, especially with the increasing threat of climate change and population increase. The study area relies heavily on groundwater for its water supply, essential for meeting industrial, agricultural, and residential needs. However, to sustain this vital resource, a thorough grasp of the groundwater potential and the variables affecting its distribution and quality is necessary. The geoelectric resistivity approach is commonly employed for groundwater exploration because of its ability to provide detailed information about the subsurface layer and its low cost of operation. Delineating Groundwater Potential Zone (GPZ) in basement terrain requires a solid comprehension of the aquifer units, and this is possible through Vertical Electrical Sounding (VES), which is typically used for groundwater research in Africa's Basement Complex rocks [6].

Many scholars have used different approaches to define Groundwater Potential Zones (GPZ) in many parts of the globe. GPZ was Characterized in Kancheepuram District, Tamil Nadu, India, using the Analytic Hierarchy Process (AHP) and the Geographic Information System (GIS) [7]. The GPZ map was categorized into five classes, varying from very high to very low. By integrating the geophysical methods of VES, Geographic Information System (GIS), and Remote Sensing (RS) techniques [8] delineate GPZ in Bankura District, India. In recent times, some researchers have also employed VES curves in conjunction with DZP for various purposes, such as identifying the GPZ of aquifers. In the Karumeniyar river basin in Southern Tamil Nadu, the VES method with DZP was Utilized to investigate aquifer productivity and delineate areas vulnerable to contamination [9]. Electrical Resistivity Tomography (ERT) and VES were used by [10] to assess leachate percolation in a contaminated waste disposal site in southeastern Nigeria; the research found that DZP effectively establishes the aquifer's protective capacity. In Karnataka, India, [11] Applied integrated VES and DZP methods to study GPZ and the protective capacity of an aquifer against surface contamination.

This study aims to appraise the groundwater potential of the studied area, the protection status of the aquifer, and proposed feasible sites for tapping groundwater using geophysical methods in conjunction with DZP and GIS techniques. The findings could be used in the sustainable management of groundwater resources both for the area under investigation and other regions with similar geological settings.

2. Study Area

Nigeria's capital, Abuja, is situated in the north-central region of the nation, generally between latitudes 8°21′ and 9°18′ N and longitudes 6′46′ and 7′37′ E. With an average elevation of 476 meters above sea level, it occupies an area of about 8000 km^2 (Figure 1). The research area experiences two distinct seasons: the dry season from November to March and the rainy season from April to October. The area's high altitude and topography's undulating characteristics directly impact the current weather. The dry season peaks in March, when average temperatures range from 30 to 37°C, with the southwest typically recording higher temperatures. Located in the Nigeria's tropical Sudan savannah region, Abuja is characterized by a combination of Sudan Savannah Vegetation and woody plant-dominated forest. With 1200 mm average annual precipitation, the evapotranspiration rate in the area is relatively high due to high tropical temperatures [12]. Nigeria's average groundwater recharge rate is less than 15% of the total rainfall, with relative variation from one catchment to another [13].

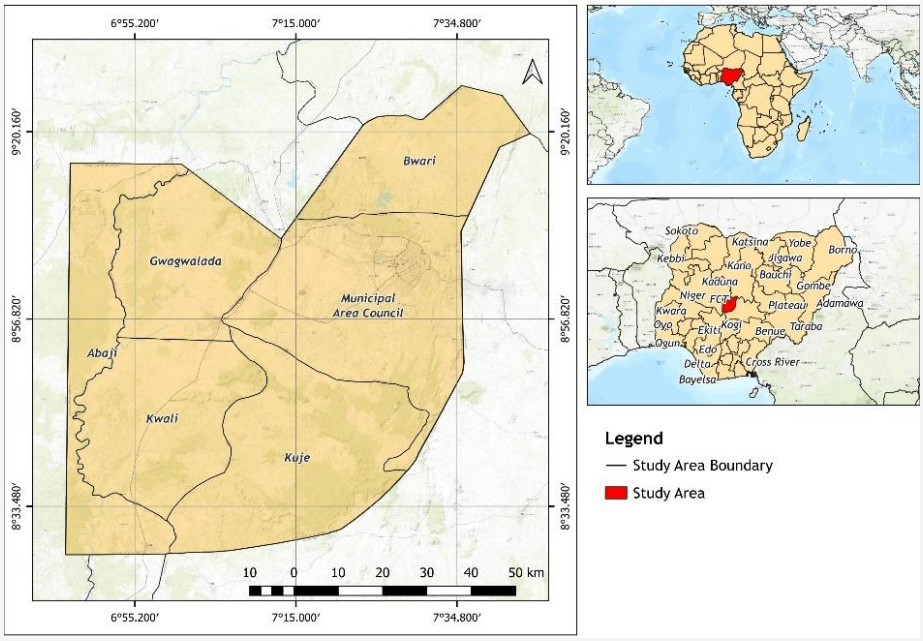

Figure 1: Location map of the study area

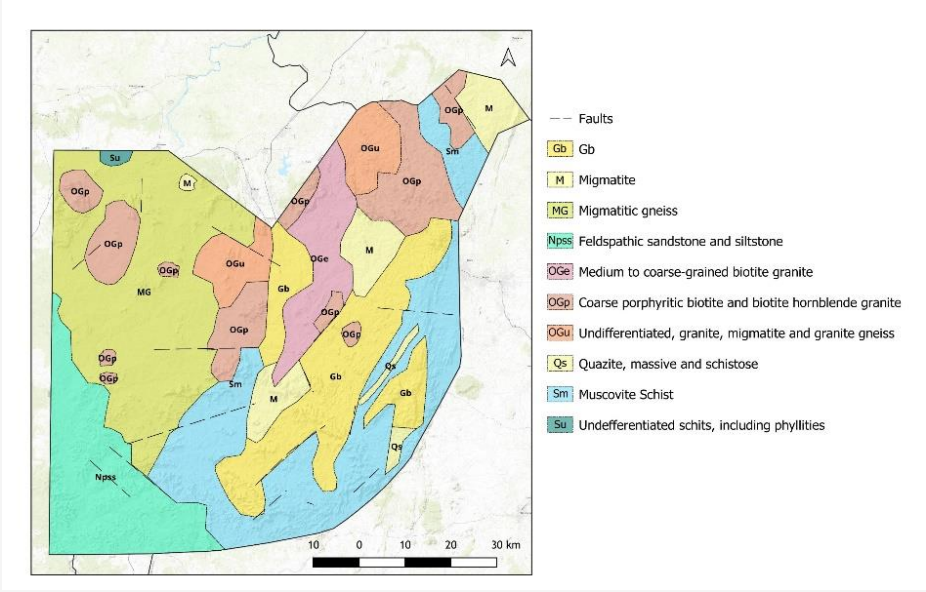

Figure 2: Geological map of the study area

2.1 Geology

The Federal Capital Territory (FCT) predominantly consists of the crystalline rocks of the North-Central Basement Complex. The observed tectonic structures have a N-S to NNE – SSW inclination resulting from the collision between the West African craton and the pan-African mobile belts during the pan-African Orogeny (Figure 2). Generally, the rock types in the study area are grouped into two: crystalline rocks (85%) and sedimentary rocks (15%).

However, the two groups were further categorized into four main groups, as reported by [15]:

1. The Migmatite-Gneiss units (Pan-African to Eburnean)
2. The Metasediments (Upper Proterozoic) comprise amphibolite, schist, phyllites, quartzites, and serpentinites, forming low-grade, metasediment-dominated belts trending north-south.

3. The older granites (Late Proterozoic) are deep-seated and typically concordant or semi-concordant within the basement complex.
4. The Upper Cretaceous sedimentary units in the Bida basin consist of a series of deposits ranging from alluvial to marine, with compositions varying from clay to gravel. These sedimentary deposits directly overlay the basement units in the tectonically controlled Bida Basin.

2.2 Hydrogeology

The conceptual hydrogeological model in tropical African countries consists of two fundamental layers: The weathered (regolith) layer and the underlying crystalline basement rocks. However, in recent research, [14] proposed a detailed model containing five layers. (i) Residual soil: which is the topmost layer, comprises laterite, pisoliths and ferralitic soils, characterized by low permeability because of high clay content. (ii) Upper saprolite: This layer is found just beneath the residual soil and is rich in secondary clay minerals with very low permeability. (iii) Lower saprolite: This layer shares similarities with the upper saprolite but exhibits increasing permeability at greater depths. It underlies the upper saprolite. (iv) Saprock: This is the fractured layer overlying the fresh bedrock. It is characterized by excellent permeability and often decreases with depth. (v) Fresh bedrock: is the bottom layer, often low in fractures, and its permeability depends principally on the rock's matrix. The lower saprolite layer and its underlying Saprock are the primary aquifer layers in the study area, as shown in Figure 3. Influenced by surface morphology, groundwater predominantly flows from the northeast to the southwest in the study area. Several factors influenced the groundwater potential in the region, which include depth to bedrock, rock type, rock composition, and the density of the fracture network. The storage capacity of the aquifer is affected by seasonal fluctuations in water table depth, which varies from one location to another. Additionally, the thickness of the weathered layer displays prominent variability within the basin, stretching up to tens of meters.

3. Materials and Method

3.1 Vertical Electrical Sounding (VES)

Vertical Electrical Sounding (VES) is a technique used to examine the Earth's subsurface using geoelectric methods. It operates on the principle that injecting current into the Earth through two electrodes along a profile line produces an electric field in the subsurface. The variation in electric potential is measurable by placing two additional electrodes properly in line with the current electrodes [16]. The apparent resistivity of the Subsurface can be determined based on the electrode spacing using different configurations, which include Schlumberger, Wenner, or a Dipole-Dipole array [17]. The choice of configuration depends on the objective of the investigation. The four measurement electrodes determine the potential difference (MN) when a current (AB) is injected between A and B. The apparent electrical resistivity obtained results from multiplying the measured electrical resistance by a coefficient influenced by the position of the four electrodes (Figure 4).

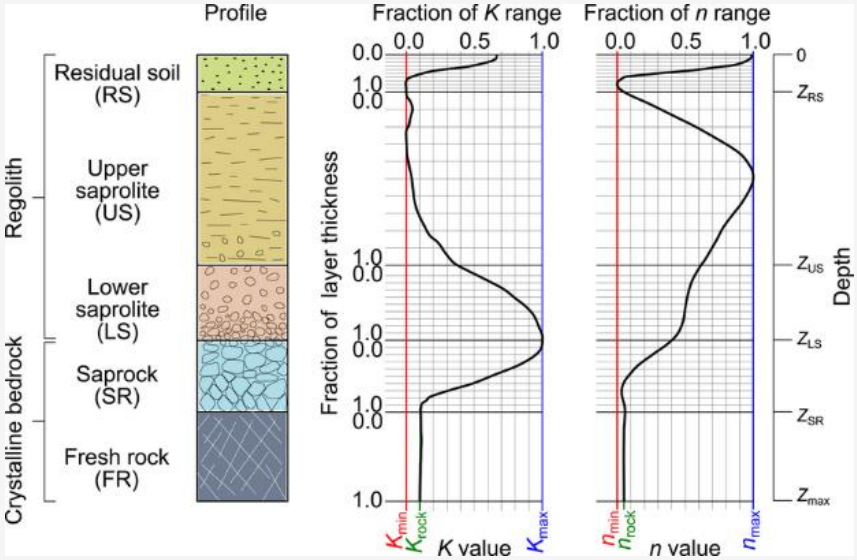

Figure 3: Conceptual model of physical heterogeneity in a weathered basement aquifer of Africa [14]

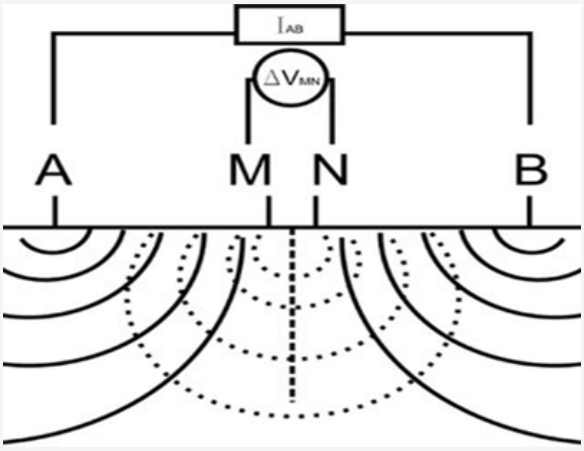

Figure 4: Vertical electrical sounding (VES) using Schlumberger array (After [19])

Using a DC Allied Ohmega resistivity meter (Campus Ohmega Ω), field resistivity data were collected in 823 locations across the FCT with a maximum current electrode separation (AB/2) of 100m, employing the Schlumberger electrode configuration (Figure 4). Vertical changes in ground resistivity with depth were measured using this configuration. The Schlumberger array was applied because it offers operational, practical, and interpretational advantages over the Wenner array [18]. The VES method employed in this research was carried out by injecting an electric current into the ground through two electrodes (AB) and measuring the consequent potential difference across two other electrodes (MN). The spacing between the electrodes widens as the central point of the electrode remains in place. But, as the current electrode gaps increase, the current penetrates vertically deeper into the subsurface, and the calculated apparent resistivity reflects the resistivity of the deeper layers.

The geospatial identities of the survey points (VES) were determined using a global positioning system (GPS) equipment. Resistance is defined as the ratio of potential difference to current in ohms (Ω). The field data obtained at each VES location were in resistance (ohms) and were transformed into apparent resistivity (ρ_a) by multiplying the resistance with a geometric factor (K), as explained below. The formular for the apparent resistivity is expressed (Equation 1):

$$\rho_a = K\frac{\Delta V}{\Delta I} \qquad \text{Equation 1}$$

Where:

ρ_a = Apparent resistivity (Ωm)
ΔV = Variation in potential
ΔI = Variation in current
K = Geometric Factor

For the Schlumberger array, The Geometric factor (K) is determined from
Equation 2 [18].

$$K = \left[\frac{\left(\frac{AB}{2}\right)^2 - \left(\frac{MN}{2}\right)^2}{\left({}^{MN}/_{2}\right)}\right] \times \pi \qquad \text{Equation 2}$$

Where:

AB = The current electrode spacing
MN = The potential electrode spacing
$\pi = \frac{22}{7}$

The apparent resistivity generally reflects the true ground resistivity in a geologically homogeneous terrain. However, in other terrains, it signifies the mean of the resistivities of all formations or layers the current has passed through. The variation in apparent resistivity in response to the change in electrode spacing measures the variability of the geoelectric layers in the subsurface.

3.2 Data Analysis and Interpretation

The field data was analyzed using computer iteration software IPI2win, which offers both automated and instruction manual interpretation of the apparent resistivity [20]. The degrees of proximity were steadily iterated between theoretical and observed VES curves until the most accurate fit was obtained. The resulting VES curves underwent smoothing to decrease the impact of lateral inhomogeneity and noisy signatures to the barest minimum. The complete VES data's Root Mean Square (RMS) error varied from 2% to 8.5%. The interpreted 1D model provides insightful subsurface information on geo-electrical layers, thickness, and depth (Table 1).

3.3 Dar Zarrouck and Hydraulic Parameters

The Dar Zarrouck parameters (DZP) are products of resistivity data; they offer valuable information regarding the composition of the subsurface layers. They are often acquired from vertical electrical sounding (VES) measurements. The two significant DZPs are Longitudinal conductance (S) and Transverse Resistance (T).

Table 1: Interpreted VES Data

VES No.	Longitude	Latitude	Curve Type	ρ_1 (Ωm)	ρ_2 (Ωm)	ρ_3 (Ωm)	ρ_4 (Ωm)	ρ_5 (Ωm)	h_1 (m)	h_2 (m)	h_3 (m)	h_4 (m)	h_5 (m)	DB (m)
S001	7.572764	8.946708	KH	110	1207	45.8	1171		0.308	0.558	1.13	46.1		48
S002	7.533836	8.927561	H	94	30.9	340			0.858	2.8	36.2			40
S003	7.425061	8.865258	KH	203	2012	103	530	3225	0.338	0.433	0.934	18.7	19	40
S004	7.221411	8.853986	H	1020	166	607			0.418	7.83	58.8			67
S005	7.560064	8.928397	KH	139	1087	51.2	201	4360	0.37	0.516	1.06	11.1	16.9	30
S006	7.55205	9.244878	KH	657	12939	1282	11479		0.434	0.341	6.47	18.8		26
S007	7.246439	8.853483	KH	68.8	1340	35.9	280		0.306	0.435	1.15	40.5		42
S008	7.239353	8.865278	HA	212	71.6	3874	232		0.942	1.36	1.88	59.6		64
S009	6.800636	8.641894	HA	413	1121	103			1.19	0.815	2.63			5
S010	7.560167	8.919739	KH	34.2	543	10.6	151		0.354	0.663	1.22	49.2		51
S212	7.020031	9.175444	H	138	138	33.9			0.503	0.754	6.81			8
S213	7.024728	9.170817	H	871	30	185			0.51	0.598	6.12			7
S214	7.013172	9.259547	H	438	438	79.6			0.323	0.485	8.81			10
S215	6.857319	9.111811	KH	93.1	1270	27.7			0.297	3.94	6.1			10
S216	7.348106	9.148697	HA	1538	1530	400			3.62	3.412	12.8			20
S217	7.324961	9.150564	H	9883	333	39.2	1777	88.1	0.18	1.24	1.71	6.67	11.4	21
S218	7.409564	9.079367	H	31225	172	45.9	792		0.155	1.28	1.29	30.4		33
S219	7.405703	9.079056	H	910	910	131	38770		0.388	0.582	4.42	10.1		16
S220	7.329908	9.151764	KH	94	349	56.4	763	54.8	0.972	1.12	2.06	4.66	10.9	20
S221	7.500844	9.102908	KH	150	1416	60.7	11191		0.416	0.641	1.05	7.31		9
S488	7.052708	8.920297	H	77.5	77.5	17.2			0.22	0.331	15			16
S489	7.566478	9.006517	KH	119	1461	27.4	1217		0.294	0.952	1.19	7.32		10
S490	7.374533	9.062047	HK	246	29.8	243	21.6		0.754	0.823	1.51	4.56		8
S491	7.098369	8.943892	H	2027	197	53.5			0.242	0.714	14.5			16
S492	7.088286	8.946708	H	506	506	46			0.282	0.423	13.3			14
S493	7.0862	8.944542	QH	1032	191	118			0.33	3.1	14.2			18
S494	7.426389	8.989169	H	440	440	111			0.442	0.662	1.73			3
S495	7.425258	8.999633	QH	404	44.7	436	18.9		0.908	1.18	2.55	5.97		11
S496	7.357997	9.137056	QH	1325	835	68.4	1886		0.847	1.68	6.67	9.38		19
S497	7.073525	8.960297	KH	386	1328	105			1.32	7.73	10.9			20
S498	7.4795	9.003458	HA	22.7	120	16.8			0.321	0.537	6.83			8
S499	7.483347	9.091603	H	256	40.3	21.3			0.412	5.35	4.4			10
S500	7.505219	9.209175	QH	126	30.5	11.8	268		0.611	2.94	5.42	7.99		17
S501	7.501889	9.206075	QH	222	2636	27.7	609		0.534	0.681	3.69	16.3		21
S813	7.629722	9.257144	H	100	50.6	12.7	747		0.633	2.66	5.5	13		22
S814	7.655128	9.316886	HA	275	549	26.8	251		0.628	0.692	1.22	15.5		18
S815	7.2437	8.686872	H	422	151	544	42.5	242	0.893	1.04	2.54	3.33	29.2	37
S816	7.338028	8.907514	QH	590	257	63.4			0.554	4.7	14.2			20
S817	7.375139	8.911894	HA	246	53.1	32.1			0.277	1.92	14			16
S818	7.367511	8.968794	H	177	14.8	63.7			0.603	0.527	7.08			8
S819	7.571214	9.221919	KH	10.7	493	9	1442		0.491	0.703	5.79	13.5		21
S822	7.286211	8.826656	HA	473	473	144			0.645	0.967	11.1			13
S823	7.358475	8.952175	QH	679	122	24			0.225	2.73	8.29			11

** The data shown here are representative values extracted from the entire dataset of 823 VES points*

However, in 1947, [21] Introduced additional parameters derived from resistivity, such as Total transverse unit resistance (*T*), longitudinal resistivity (ρl), transverse resistivity (ρt), and the coefficient of anisotropy (λ) in addition to the longitudinal conductance (*S*). These parameters play a critical role in subsurface hydrogeology; their importance was explained by various authors [22, 23 & 24] in different regions.

3.3.1 Longitudinal conductance

The longitudinal conductance, denoted as *S*, is defined as the ratio of layer thickness to the corresponding layer resistivity. Longitudinal conductance (*S*) was obtained from VES data in the study area, and the total longitudinal conductance was calculated using Equation 3. Table 2. Represent some parts of the outcomes.

$$S = \sum_{i=1}^{n} \frac{h_i}{\rho_i}$$

Equation 3

Where:

h_i = Thickness (m)
ρ_i = Resistivity (Ωm)

The value of "*S*" serves as an indicator of basement depth and aquifer transmissivity. A high "*S*" value suggests a deeper basement and low aquifer transmissivity, while a low "*S*" value suggests a shallower basement and good transmissivity [25].

Locations with low "*S*" values are favorable for groundwater development.

3.3.2 Transverse Resistance (T)

The transverse resistance is calculated by multiplying a layer's true resistivity by its corresponding thickness. To determine the relationship between transmissivity and groundwater flow, the transverse unit resistance (T) has to be evaluated. Underground geological formations are characterized based on their resistivity and thickness. The direction of groundwater flow in an aquifer can also be determined using the transverse unit resistance. High T values indicate high transmissivity in any given aquifer [24]. The T in the study area was calculated using the formula below (Equation 4):

$$T = \sum_{i=1}^{n} \rho_i h_i$$

Equation 4

Where:

h_i = Thickness (m)
ρ_i = Resistivity (Ωm)

A high value of T in a specific area indicates higher transmissivity, as highlighted by [26]. Greater transmissivity suggests favorable locations for groundwater development.

3.3.3 Coefficient of electrical anisotropy

Electrical anisotropy coefficient (λ) measures how the electrical resistivity of subsurface geological materials changes in different directions. It helps quantify the extent of anisotropy in the electrical properties of subsurface layers. It evaluates the degree of heterogeneity in subsurface Hard rock terrain. Primary and Secondary structural signatures like joints, foliation, faults, bedding planes, and fractures are generally influenced by it. Other factors include the near-surface effect and the degree of weathering [27]. The coefficient of anisotropy (λ) was calculated using the equation below Equation 5:

$$\lambda = \sqrt{\frac{T_A}{S_A}}$$

Equation 5

Where:

λ = Coefficient of electrical anisotropy
T_A = Average transverse resistivity
S_A = Average longitudinal resistivity

3.3.4 Reflection Coefficients (R_c)

The response of the subsurface geological layers to electric current passing through them is called its reflection coefficient. This parameter is used to understand the changes in resistivity between distinct geological layers and plays a vital role in determining the groundwater potential (GP) of a given area. The reflection coefficients (R_c) of the study area was evaluated using the method proposed by [28] as shown in Equation 6:

$$R_C = \frac{\rho_n - \rho_{n-1}}{\rho_n + \rho_{n-1}}$$

Equation 6

Where:

R_C = The reflection coefficient
ρ_n = The nth layer resistivity
ρ_{n-1} = The resistivity of the layer overlying the nth layer

3.4 Aquifer Vulnerability Assessment

Groundwater is recharged by rainfall or other surface water sources; sometimes, this source of recharge becomes contaminated due to natural or anthropogenic activities. The ability of the geologic material to filter out these contaminants during percolation is called its protective capacity. To assess the vulnerability of the aquifer in the study area, longitudinal conductance (*S*) values were used. S is directly related to the textural ability of the earth's material to protect against infiltrating pollutants. This evaluation is based on the aquifer's protective capacity rating proposed by [29] (Table 3).

3.5 Groundwater Potential Zone Mapping

The resistivity signature of a subsurface geological material alone cannot be reliable in determining the GPZ of a given area; reflection coefficient (R_C) is an important parameter in delineating GPZ. A lower R_C (less than 0.8) indicates a highly weathered or fractured bedrock, signifying a high GP. Areas characterized by significant depth to bedrock and low reflection coefficient (<0.8) indicate a promising GPZ. GP of the FCT was delineated using *DB* and R_C obtained from the interpreted VES data following a modified fundamental criteria applied by [30]:

- Very High Groundwater Potential: Areas with $DB \geq 30$m and $R_C < 0.8$
- High Groundwater Potential: Areas with $DB \geq 13$m and $R_C < 0.8$
- Moderate Groundwater Potential: Areas with $DB \geq 13$m and $R_C \geq 0.8$
- Low Groundwater Potentials: Areas with *DB* of < 13m and $R_C > 0.8$
- Very-low groundwater Potential: Locations with $DB < 13$m and $R_C < 0.8$

The research area was characterized into five measurable GPZ based on the above-mentioned criteria, and a groundwater potential map was generated [29].

Table 2: Groundwater Potential, Protective Capacity, and Dar Zarrouck Parameters

VES No.	Longitudinal Conductance	Protective Capacity	Depth to Bedrock (m)	Reflection Coefficient	Groundwater Potential (GP)	Transverse Resistance	Coefficient of Anisotropy
S001	0.067302854	Poor	48	0.924720579	Moderate	54742.24	1.262028
S002	0.206213135	Moderate	40	0.833378269	Moderate	12475.17	1.272524
S003	0.052122686	Poor	40	0.71770972	Very High	72222.01	1.55703
S004	0.14444833	Weak	67	0.570504528	Very High	37417.74	1.096501
S005	1.079063577	Good	30	0.911861434	Moderate	76581.69	2.661368
S006	0.007371508	Poor	26	0.799075308	High	228797.1	1.576809
S007	0.181448585	Weak	42	0.772712884	Very High	11985.24	1.100086
S008	0.280819648	Moderate	64	-0.886994642	Very High	21407.4	1.215619
S009	0.029142366	Poor	5	-0.831699346	Very Low	1675.975	1.507809
S010	0.452494026	Moderate	51	0.868811881	Moderate	7814.248	1.156044
S110	0.247425881	Moderate	20	-0.631299735	High	3087.428	1.409214
S111	0.046799605	Poor	9	-0.888717156	Very Low	5347.11	1.700974
S112	0.070734035	Poor	13	0.972454501	Moderate	38408.75	4.008227
S113	0.225117548	Moderate	22	-0.520833333	High	2418.816	1.056452
S114	0.398280877	Moderate	12	-0.854616896	Very Low	930.009	1.62139
S115	0.150980352	Weak	8	-0.65203252	Very Low	867.118	1.205429
S116	0.314042276	Moderate	19	-0.82084452	High	3273.964	1.710862
S117	0.049729307	Poor	10	-0.930886456	Very Low	8751.255	2.155093
S118	0.311209721	Moderate	15	-0.775373847	High	1305.781	1.329727
S119	0.194543649	Weak	25	-0.438256659	High	3600.389	1.070835
S120	0.423277386	Moderate	7	-0.843398876	Very Low	396.4416	1.861199
S300	0.233859112	Moderate	7	-0.66970618	Very Low	940.192	2.246681
S301	0.056221825	Poor	22	0.622641509	High	10838.1	1.139648
S302	0.02412832	Poor	3	-0.861122896	Very Low	739.1755	1.565872
S303	0.016613025	Poor	3	-0.759364359	Very Low	1582.185	1.532699
S304	0.10513933	Weak	19	0.930004093	Moderate	20671.98	2.509563
S305	0.041668401	Poor	14	0.993724787	Moderate	301355.4	7.975658
S306	0.06566597	Poor	9	-0.394117647	Very Low	1791.866	1.149325
S307	0.162641937	Weak	21	0.912988849	Moderate	11942.58	2.07839
S308	0.682493596	Moderate	20	-0.784386617	High	1492.108	1.600625
S309	0.068169066	Poor	8	-0.780104712	Very Low	2537.46	1.73739
S310	0.075417485	Poor	9	-0.467336683	Very Low	1262.404	1.079719
S630	0.673010057	Moderate	30	0.896972795	Moderate	4425.249	1.802524
S631	0.317069152	Moderate	25	0.904992729	Moderate	7156.778	1.917715
S632	0.358478789	Moderate	28	-0.559251559	High	3306.459	1.218393
S633	0.342700033	Moderate	18	-0.769082392	High	2091.888	1.529989
S634	0.127765757	Weak	29	-0.868613139	High	7952.967	1.08857
S635	0.571607348	Moderate	12	-0.432900433	Very Low	1296.706	2.248523
S636	0.100412117	Weak	12	-0.509513742	Very Low	1472.523	1.022256
S637	0.387171404	Moderate	19	-0.825805222	High	1537.5	1.279473
S638	0.380854843	Moderate	13	-0.743190661	High	516.212	1.081654
S820	0.566258253	Moderate	26	-0.835577605	High	1339.93	1.048548
S821	0.247539954	Moderate	11	-0.833280102	Very Low	1552.765	1.786205
S822	0.080491367	Poor	13	-0.533225284	High	2360.876	1.08442
S823	0.368125086	Moderate	11	-0.671232877	Very Low	684.795	1.411947

The data shown here are representative values extracted from the entire dataset of 823 VES points

Table 3: Aquifer protective capacity rating [29]

Longitudinal Conductance (S)	Protective Capacity
>10	Excellent
5 - 10	Very good
0.7 – 4.9	Good
0.2 – 0.69	Moderate
0.1 – 0.19	Weak
<0.1	Poor

3.6 Geospatial Analysis

Ordinary Kriging (OK) interpolation algorithm was used to generate the groundwater potential map, Aquifer vulnerability map, and other related parameters using the smart-map QGIS plugin. Smart-Map is a QGIS plugin that allows the generation of interpolated maps; the plugin is registered with the National Institute of Industrial Property (INPI, Ministry of Economy, Brazil, BR 51 2021 000002-1) [31] (https://plugins.qgis.org/plugins/Smart_Map). To achieve a finer resolution image and reduce the Computational time, the pixel size of each thematic layer was set to 100 meters.

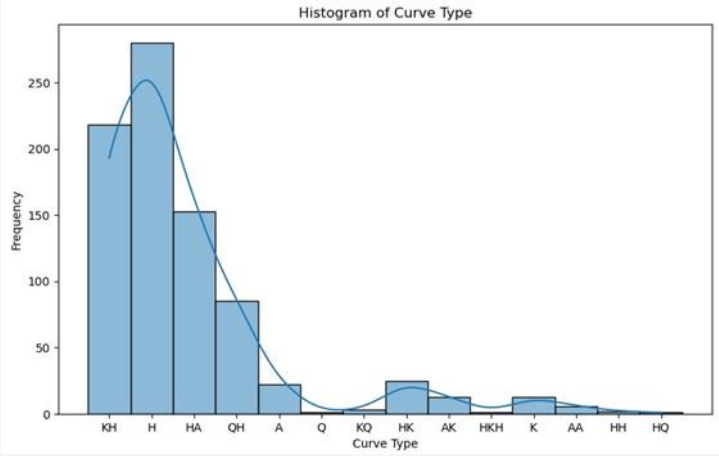

Figure 5: Curve-type distribution across the study area

(a)

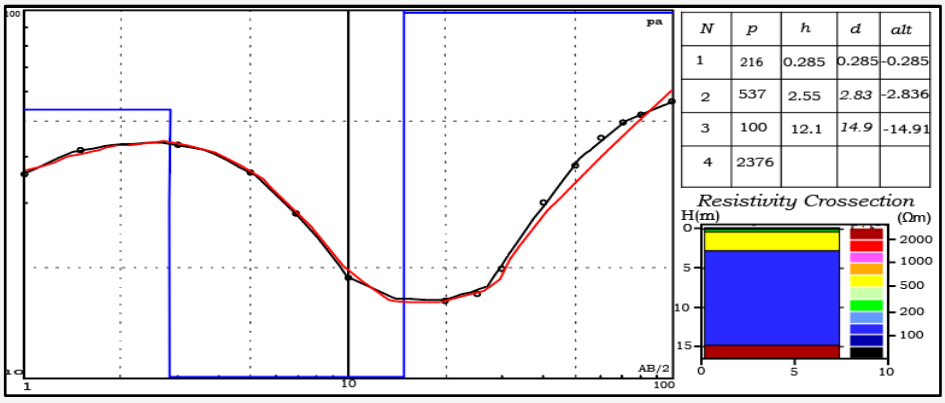

(b)

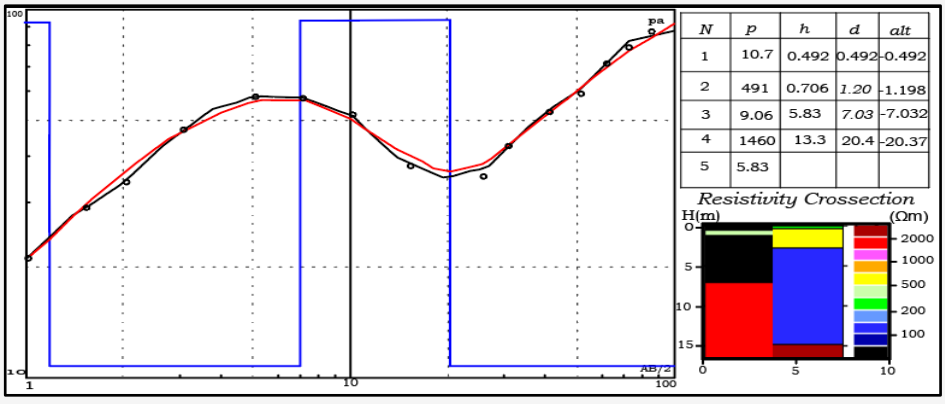

Figure 1: Shows the two most dominant curve-type across the study area:
(a) Typical H-type Curve and (b) Typical KH-type Curve

The output of the analysis was typically in a continuous raster format. However, the quantile-break points classification mode was used to obtain a categorical raster map. The choice of using quantiles was made because they best represent the analysis output in relation to the Hydrogeological conditions of the study area. Kriging is an unbiased linear interpolation technique that uses a weighted average of nearby samples to estimate unknown values in specific areas. It is deemed the best interpolation method for spatially varying data. For this study, the resistivity data was randomly distributed over a large area, and the sampling distance between one VES data and the other ranged from 0.5km to 10km. A careful choice of analytic tool is therefore needed to interpolate the dataset.

4. Result and Discussion

4.1 VES Data Analysis and Interpretation

Typical curve types observed in the field from the 823 VES data collected across the study area are shown in Figure 6. The result from the interpreted VES shows that the dominant curve type is the H-type (34%) curve, followed by the KH-type (26.5%) and then HA-type (18.6%) other curve types with reasonable dominance in the study area were the QH (10.3%), HK (3.0%), A (2.7%), K (1.6%), AK (1.6%) and AA-type (0.7%). VES curve-type distribution frequencies are showcased in Figure 5. The summary result of the study area's subsurface resistivity and layer thickness values is presented in Table 1. A reasonable percentage of the VES data displays three geoelectric layers (52%), followed by those with Four (39.4%) and five (8.5%) layers, respectively.

The maximum value of the first layer resistivity is 180001Ωm while the minimum value is 0.309Ωm, and the average resistivity value is 1808Ωm. The first layer VES point with the highest value is located around the central part of the FCT (Gada Biyu), a transition zone between the Basement terrain and the sedimentary formation. The second layer resistivity has a maximum value of 27685Ωm, a minimum value of 1.16Ωm, and an average resistivity value of 605Ωm. The third layer has a maximum resistivity value of 42256Ωm and a minimum of 0.788Ωm. The average resistivity across the entire third layer is 650Ωm. In terms of layer thickness, the maximum thickness of the first, second, and third layers are approximately 6,18 and 78m, respectively. The spatial interpolation map of the thickness and resistivity layers of the first and third layers are represented in Figure 7.

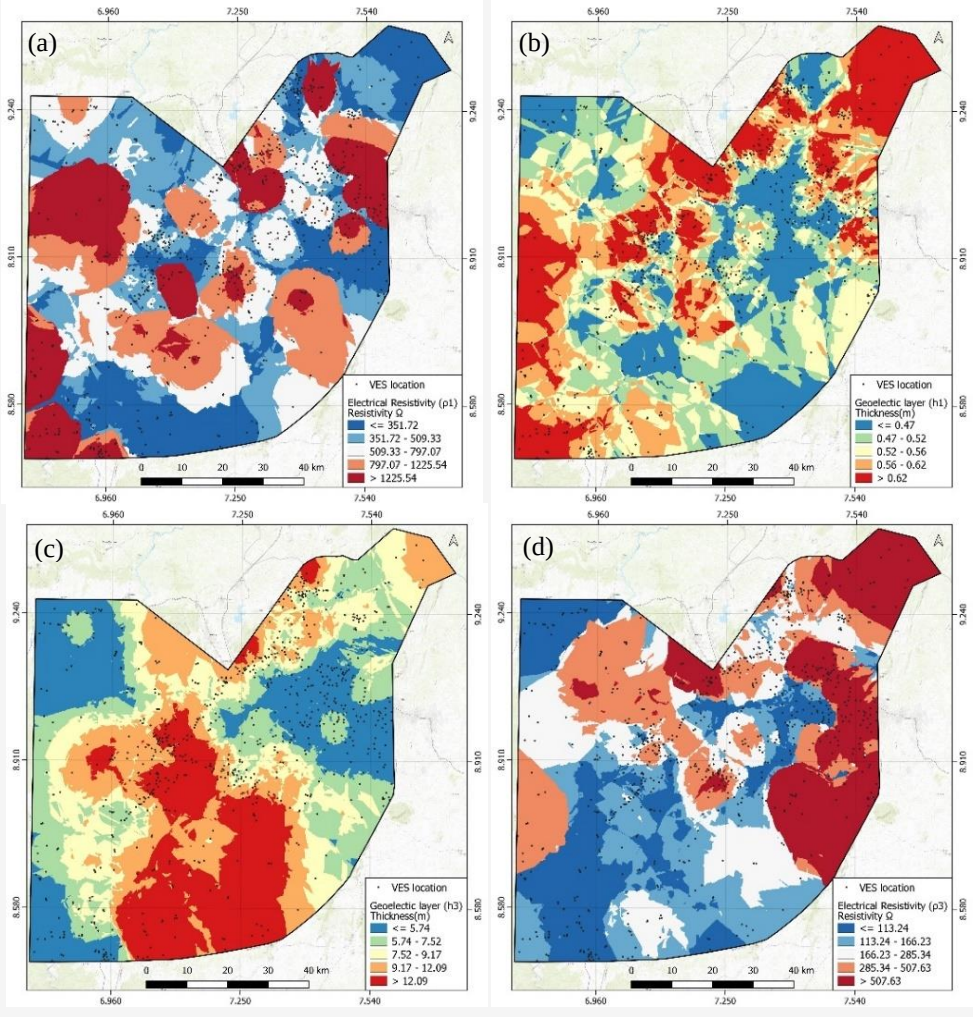

Figure 7: Layer Properties: (a) Spatial distribution of the first layer resistivity (b) First layer thickness (c) Third Layer thickness (d) Third layer resistivity

4.2 Geoelectric Section

From the VES data analysis, the geoelectric layers detected in the study area range from three to five layers. The topsoil is the upper layer rich in silt, clayey-sand, and sand. It shows a resistivity varying from 0.309 to 180001Ωm and a thickness of 0.036 to 5.6m. The topsoil plays a crucial role in the groundwater recharge mechanism by enabling surface water infiltration into the aquifer. Hydrogeologically, the topsoil comprises three parts: the soil water zone at the top, followed by the vadose zone, and the capillary margin at the bottom. The variation in their resistivity values is ascribed to the differences in compaction of the clayed sand. The second layer is the weathered zone with resistivity values ranging from 1.16 to 27685Ωm and an average resistivity of 604Ωm. The average thickness of this layer across the study area is 2.07m. This layer is made up of the by-products of weathering. It comprises laterite, alluvial deposits, saprolite, clays, and sometimes partly fractured rocks. In hydrogeological studies, this zone is critical because it plays a role in groundwater storage and movement. The shallow aquifer is easily accessible and are commonly exploited through hand-dug wells. The third layer is the fractured basement, and it hosts the main aquiferous unit in the region. The resistivity of this layer ranges from 0.788 to 42256Ωm with a maximum thickness of 78m and an average thickness of 9m.

4.3 Depth to Bedrock

One of the best methods of delineating overburden thickness or depth to bedrock, as well as the depth of fractured or weathered zones with rational precision, is through the electrical resistivity method [32]. A clear understanding of *DB* is critical when determining the location and depth of overlying aquifers because groundwater is often found in the weathered layer overlying the bedrock or fractures and joints within the bedrock. The depth to bedrock in the study area ranges from 1 to 86m, and the average depth to bedrock is 18.6m. Areas with the deepest *DB* are in the SW to SE part of the study area and host the most promising aquifers. Figure 8(a) shows the spatial distribution of depth to bedrock.

4.4 Aquifer Vulnerability Map

The aquifer protective capacity of the study area is directly linked to the longitudinal conductance; this is shown in the Summary (Table 2). The spatial distribution of the FCT aquifer protective capacity indicates that the area is moderately protected against surface contamination, as represented in the aquifer vulnerability map Figure 8(b).

4.5 Groundwater Potential Zone Evaluation

Tectonic history, weathering activities, groundwater flow patterns, and the intricate interaction of geological factors determine the GP in the basement terrain. Depth to bedrock and lower reflection coefficient increased the GP in some parts of the basement complex in Nigeria [33].

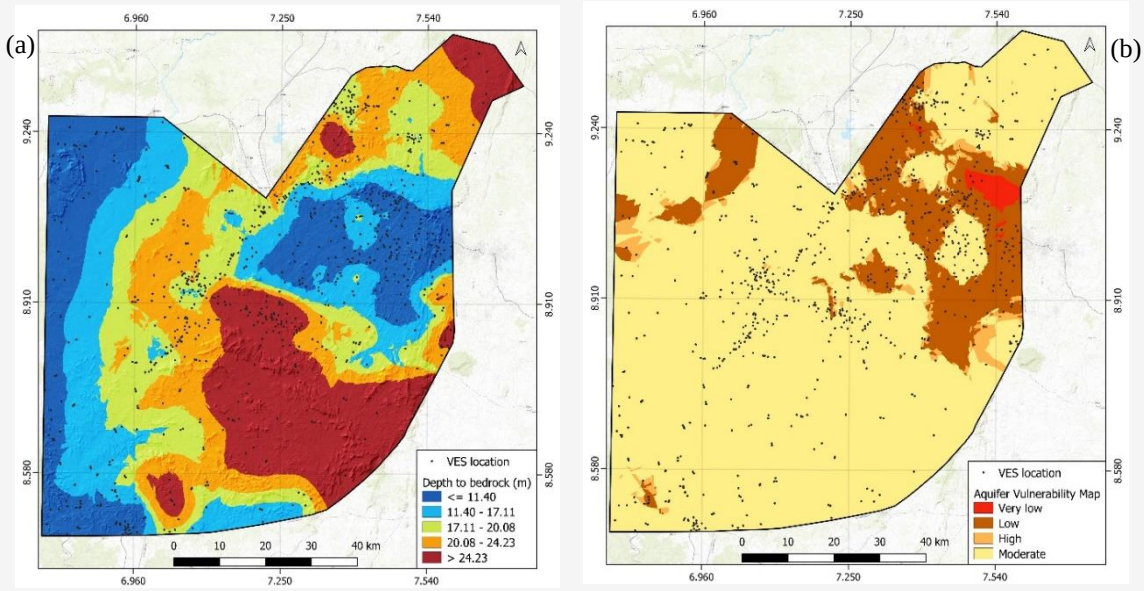

Figure 8: (a) Spatial distribution of depth to bedrock across the study area
(b) Aquifer Vulnerability map of the study area

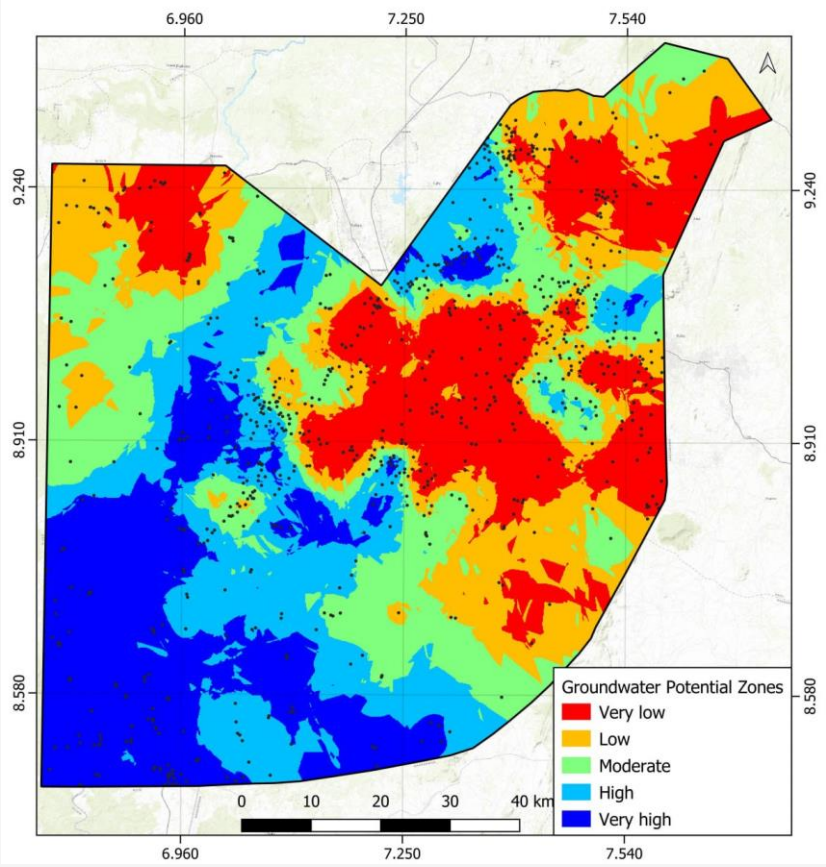

Figure 9: Groundwater potential zone map of the study area

The Study area's GP was evaluated based on the aquifer geoelectric parameters extracted from the VES data. The GPZ map of the study area was created from the data partially represented in Table 2. Based on the primary criteria mentioned earlier, the region was divided into five zones: Very High. High, Moderate, low, and Very Low groundwater potential zone (Figure 9).

5. Conclusion

This paper presents the results from a Hydrogeophysical investigation of groundwater potential and evaluation of the aquifer vulnerability of FCT using the electrical resistivity method and geospatial techniques; 823 vertical electrical sounding (VES) data using the Schlumberger configuration were processed to identify potential groundwater zones in the study area. The VES data displays three to five subsurface layers, with H, KH, HA, and QH. Dominating the sounding curve-types respectively. The apparent resistivity measurements acquired varied from 0.309Ωm to 180001Ωm with an average value of 1170Ωm. The subsurface geoelectric characteristic of the study area was understood using the VES techniques.

The result reveals the significance of alluvial deposits, sandy and clayey layers in sedimentary terrain, and weathered and fractured bedrock in basement terrain for groundwater storage and transmission. Remarkably, in the hard rock part of the study area, the integration of low resistivity and a reasonable depth to bedrock contribute to good aquifer formation. The region was classified into five distinct groundwater potential zones: Very High (19.7%), High (20.3%), Moderate (20%), Low (20%), and Very Low (20%), using the reflection coefficient and aquifer thickness (*DB*). The Vulnerability map of the area was created from the protective capacity evaluation, indicating that the area is broadly moderately vulnerable. Proper grouting is therefore recommended after Borehole drilling. Spatial interpolation using the Kriging methodology was employed to display the spatial distribution of layer resistivity, layer thickness, aquifer vulnerability, and the groundwater potential of the area. The southwestern part of the study area, which is broadly sedimentary terrain, has the highest groundwater potential as evidenced from the findings of the study.

Stakeholders in water resources management will make informed decisions from the findings of this research. Developing a 3D model that will incorporate various resistivity layers and evaluating the model using borehole data and pumping test analysis to confirm the identified potential zones is one prospective area for future research.

Acknowledgments

This research work was graciously supported by SPRING (Support for Pioneering Research Initiated by the Next Generation) under the auspices of Osaka Metropolitan University (OMU), Osaka, Japan. My profound gratitude goes to the Department of Geosciences OMU for providing a conducive environment for the research and to my supervisors for their guidance and mentorship.

References

[1] Naghibi, S. A., Pourghasemi, H. R. and Dixon, B., (2016). GIS-based Groundwater Potential Mapping Using Boosted Regression Tree, Classification and Regression Tree, And Random Forest Machine Learning Models in Iran. *Environmental Monitoring and Assessment*, Vol. 44. https://doi.org/10.1007/s10661-015-5049-6.

[2] MacDonald, A. M., (2005). *Intermediate Technology Development Group, Great Britain (eds) Developing Groundwater: A Guide for Rural Water Supply*. ITDG Pub, Bourton-on-Dunsmore, Warwickshire.

[3] Ajaykumar, K., Vasant, M., Wagh, S., Narayan, P. and James, J., (2021). Seasonal Variation in Groundwater Quality and Beneficial Use for Drinking, Irrigation, and Industrial Purposes from Deccan Basaltic Region, *Western India*, Vol 28, 26082–26104. https://doi.org/10.1007/s11356-020-12115-x.

[4] JICA., (2014). *The Project for Review and Update of Nigeria National Water Resources Master Plan*. 1-144. https://openjicareport.jica.go.jp/pdf/12146544.pdf.

[5] Aish, A., (2022). Estimation of Spatial Groundwater Recharge and Surface Runoff in the Gaza Coastal Aquifer Using GIS-Based WetSpass Model. *International Journal of Geoinformatics*, Vol. 18(6), 25–32. https://doi.org/10.52939/ijg.v18i6.2457.

[6] Oloruntola, O. and Adeyemi, G. O., (2014). Geophysical and Hydrochemical Evaluation of Groundwater Potential and Character of Abeokuta Area, Southwestern Nigeria. *Journal of Geography and Geology*, Vol. 6(3). https://doi.org/10.5539/jgg.v6n3p162.

[7] Tazi, M., El Azzab, D., El Moutaouakkil, N., and Charroud, M. (2024). Integration of Geospatial Technologies and Fuzzy-AHP Analysis to Assess Groundwater Potential in the Sirwa Massif, Anti-Atlas Region, Morocco. *International Journal of Geoinformatics*, Vol. 20(5), 79–94. https://doi.org/10.52939/ijg.v20i5.3235.

[8] Das, S., (2017). Delineation of Groundwater Potential Zone in Hard Rock Terrain in Gangajalghati Block, Bankura District, India Using Remote Sensing and GIS Techniques. Model Earth Syst Environ, Vol. 3, 1589–1599. https://doi.org/10.1007/s40808-017-0396-7.

[9] Al-Sababhah, N. (2023). The Application of the Analytic Hierarchy Process and GIS to Map Suitable Rainwater Harvesting Sites in (Semi-) Arid Regions in Jordan. *International Journal of Geoinformatics*. Vol. 19(3), 31–44. https://doi. org/10.52939/ijg.v19i3.2601.

[10] Udosen, N. I., (2022). Geo-Electrical Modeling of Leachate Contamination at a Major Waste Disposal Site in South-Eastern Nigeria. *Modeling Earth Systems and Environment*, Vol. 8, 847–856. https://doi.org/10.1007/s40808-021-01120-9.

[11] Vaddadi, N., Vansarochana, C., and Raghavan, V. (2022). Estimation of Groundwater Recharge Potential using Rooftop Rainwater Harvesting: Case Study from Pune Urban Area, India. *International Journal of Geoinformatics*, Vol. 18(2), 55–69. https://journals.sfu.ca/ijg/index.php/journal/article/view/2153.

[12] Handbook, F. C. T., (1994). *Federal Capital Territory, Abuja: Background, History, and Progress.* Garkida Press Limited, Abuja, Nigeria.

[13] Ashaolu, E. D., Olorunfemi, J. F., Ifabiyi, I. P., Abdollahi, K. and Batelaan, O., (2020). Spatial and Temporal Recharge Estimation of the Basement Complex in Nigeria, West Africa. *Journal of Hydrology: Regional Studies*, Vol. 27. https://doi.org/10.1016/j.ejrh.2019.100658.

[14] Bianchi, M., MacDonald., A. M., Macdonald, D. M. J. and Asare, E. B., (2020). Investigating the Productivity and Sustainability of Weathered Basement Aquifers in Tropical Africa Using Numerical Simulation and Global Sensitivity Analysis. *Water Resources Research*, Vol. 56(9), https://doi.org/10.1029/2020WR027746.

[15] Dada, S. S., (2008). Proterozoic Evolution of the Nigeria - Boborema Province. *Geological Society, London, Special Publications*, Vol. 294, 121–136. https://doi.org/10.1144/SP294.7.

[16] Zohdy, A. A. R., Eaton, G. P. and Mabey, D. R., (1974). *Application of Surface Geophysics to Ground-Water Investigations*. https://doi.org/10.3133/twri02D1.

[17] Bhimasankaram, V. L. S. and Gaur, V. K., (1977). Lectures on Exploration Geophysics for Geologists and Engineers. Association of Exploration Geophysicists, Hyderabad, India. https://doi.org/1016/0016-7142(79)90027-9.

[18] Barounis, N. and Karadima, K., (2011). Application of Half Schlumberger Configuration for Detecting Karstic Cavities and Voids for a Wind Farm Site in Greece. *Journal of Earth Sciences and Geotechnical Engineering*, Vol. 1(1), 101- 116.

[19] Laaraj, F., Benabdelhadi, M., Chibout, M., Lahrach, A. and Benslimane, A. (2023). Geophysical Study for the Recognition of the Water Resources of the Turonian Aquifer in the Eastern Part of the Boudnib Basin (Errachidia-Morocco). *Ecological Engineering and Environmental Technology*, Vol. 24(3), 79-89. https://doi.org/10.12912/27197050/157111.

[20] Bobachev, C., (2002). IPI2Win: A Windows Software for an Automatic Interpretation of Resistivity Sounding Data. PhD Thesis, Moscow State University, Russia.

[21] Maillet, R., (1947). The Fundamental Equations of Electrical Prospecting. *Geophysics*, Vol 1, 529–556. https://doi.org/10.1190/1.1437342.

[22] Henriet, J. P., (1976). Direct Applications of the Dar Zarrouk Parameters in Ground Water Surveys. *Geophysical Prospect*, Vol. 24, 344-353. https://doi.org/10.1111/j.1365-2478.1976.tb00931.x.

[23] Utom, A. U., Odoh, B. I. and Okoro, A. U., (2012). Estimation of Aquifer Transmissivity Using Dar Zarrouk Parameters Derived from Surface Resistivity Measurements: A Case History from Parts of Enugu Town (Nigeria). Journal of Water Resource and Protection, Vol. 04(12), 993–1000. https://doi.org/10.4236/jwarp.2012.412115.

[24] Niwas, S. and Singhal, D. C., (1985). Aquifer Transmissivity of Porous Media from Resistivity Data. *Journal of Hydrology*, Vol. 82, 143–153. https://doi.org/10.1016/0022-1694(85)90050-2.

[25] Srinivasa, Y., Hudson Oliver, D., Stanley, R. A., Muthuraj, D. and Chandrasekar, N., (2012). Estimation of Conductance Anomalies in Subsurface through Dar-Zarrouk Parameters by Resistivity Inversion Method. *International Journal of Physical and Mathematical Sciences*. Vol. 3(1). 140-151.

[26] Gaikwad, S., Pawar, N. J., Bedse, P., Wagh, V. and Kadam, A., (2022). Delineation of Groundwater Potential Zones Using Vertical Electrical Sounding (VES) in a Complex Bedrock Geological Setting of the West Coast of India. *Modeling Earth Systems and Environment*, Vol. 8, 2233–2247. https://doi.org/10.1007/s40808-021-01223-3.

[27] Maliek, S. B., Bhattacharya, D. C. and Nag, S. K., (2003). Behavior of Fractures in Hard Rocks - A Study by Surface and Radial VES Methods. Geoexploration, Vol. 21(3), 181-189. https://doi.org/10.1016/0016-7142(83)90063-7.

[28] Bhattacharya, P. K. and Patra, H. P. (1968). *Direct Current Geoelectric Sounding Methods*. Methods in Geochemistry and Geophysics, Vol. 9, 1-135.

[29] Oladapo, M. I. and Akintorinwa, O. J., (2007). Hydrogeophysical Study of Ogbese Southwestern Nigeria. *Global Journal of Pure and Applied Sciences*, Vol. 13. https://doi.org/10.4314/gjpas.v13i1.16669.

[30] Arunbose, S., Srinivas, Y. and Rajkumar, S., (2021). Efficacy of Hydrological Investigation in Karumeniyar River Basin, Southern Tamil Nadu, India Using Vertical Electrical Sounding Technique: A Case Study. MethodsX, Vol. 8. https://doi.org/10.1016/j.mex.2021.101215.

[31] Pereira, G., W., Valente, D., S., M., Queiroz, D., M., Freitas C., A., L., Costa, M., M., and Grift, T. (2022). Smart-Map: An Open-Source QGIS Plugin for Digital Mapping Using Machine Learning Techniques and Ordinary Kriging. Agronomy. Vol. 12; 1350. https://doi.org/10.3390/agronomy12061350.

[32] Zohdy, A. A., Jackson, D. B., Mattick, R. E. and Peterson, D. L., (1969). *Geophysical Surveys for Groundwater at White Sands Missile Range, New Mexico*. United States Geological Survey, 1-31. https://doi.org/10.3133/ofr69326.

[33] Olorunfemi, M. O. and Olorunniwo, M. A., (1985). Geoelectric Parameter and Aquifer Characteristics of Some Parts of Southwestern Nigeria. *Journal of Mining and Geology*, Vol. 2, 99–109.